Am J Transl Res 2026;18(5):4248-4264
www.ajtr.org /ISSN:1943-8141/AJTR0172320

Original Article

Single-nucleus transcriptomics identifies SPON1 as a candidate mediator of the anti-fibrotic effect of *Abelmoschus manihot* (L.) in diabetic kidney disease

Chaoyu Zhu[1], Zhen Zhu[2], Renjie Wang[3], Yuanyuan Xiao[1], Qianqian Wang[1], Xinyi Wang[1], Jun Yin[1], Li Wei[1]

[1]Department of Endocrinology and Metabolism, Shanghai Sixth People's Hospital Affiliated to Shanghai Jiao Tong University School of Medicine, Shanghai Clinical Center for Diabetes, Shanghai Diabetes Institute, Shanghai Key Laboratory of Diabetes Mellitus, Shanghai 200233, China; [2]Department of Respiratory Medicine, Shanghai Sixth People's Hospital Affiliated to Shanghai Jiao Tong University School of Medicine, Shanghai 200233, China; [3]School of Basic Medicine, Chongqing Medical University, Chongqing 400016, China

Received February 27, 2026; Accepted April 13, 2026; Epub May 15, 2026; Published May 30, 2026

Abstract: Objectives: This study elucidated the cell-type-specific mechanisms and molecular targets underlying the anti-fibrotic effects of *Abelmoschus manihot* (AM) extract in diabetic kidney disease (DKD). We focused on identifying fibrosis-associated regulators using single-nucleus RNA sequencing (snRNA-seq) and validating them experimentally. Methods: DKD was induced in C57BL/6J mice by a high-fat diet and streptozotocin. Mice received oral AM extract (2.0 g/kg/day) for 14 weeks. We performed snRNA-seq on control, DKD, and AM-treated kidneys, utilizing computational tools to infer intercellular communication. Validation was conducted using quantitative real-time polymerase chain reaction (qRT-PCR), immunohistochemistry, western blotting, and confocal microscopy. *In vitro*, human renal proximal tubular epithelial (HK-2) cells were exposed to high glucose (HG) with or without AM treatment. Results: AM significantly reduced the urinary albumin-to-creatinine ratio and ameliorated glomerular and interstitial fibrosis in DKD mice. snRNA-seq identified proximal tubular segment 1 and interstitial cell clusters as the primary responders to AM. The extract suppressed transforming growth factor-beta TGF-β/Smad-related profibrotic signaling and remodeled epithelial-stromal intercellular communication by downregulating C-X-C motif chemokine ligand (CXCL) and colony-stimulating factor (CSF) pathways. Notably, spondin 1 (SPON1), an extracellular matrix-associated matricellular protein, was among the most significantly downregulated genes. Consistent with these findings, SPON1 expression was markedly reduced in both DKD kidneys and HG-injured HK-2 cells following AM administration. Conclusions: AM attenuates diabetic renal fibrosis by reducing SPON1 expression, suppressing profibrotic signaling, and remodeling epithelial-stromal crosstalk. These findings provide cell-type-resolved insights into AM's renoprotective mechanisms and highlight SPON1 as a candidate molecular target in DKD.

Keywords: *Abelmoschus manihot* (L.), diabetic kidney disease, renal fibrosis, SPON1, single-nucleus RNA sequencing, epithelial-stromal interaction

Introduction

The global prevalence of diabetes mellitus continues to rise at an alarming rate, currently affecting an estimated 537 million adults worldwide [1]. Diabetic kidney disease (DKD) is a major chronic complication of diabetes and a leading cause of chronic kidney disease (CKD) and end-stage renal disease (ESRD). It affects 20-40% of individuals with diabetes and accounts for most ESRD cases in many regions [2]. The pathologic hallmarks of DKD include persistent albuminuria, a progressive decline in the glomerular filtration rate (GFR), glomerulosclerosis, and tubulointerstitial fibrosis. These features collectively lead to irreversible loss of renal function and patient morbidity [3].

Despite therapeutic advances, including renin-angiotensin system (RAS) inhibitors [4], sodium-glucose cotransporter-2 (SGLT2) inhibitors [5], and mineralocorticoid receptor antagonists (MRAs) [6], a significant number of patients continue to experience residual albuminuria

https://doi.org/10.62347/BNGC7471

and progressive kidney fibrosis. Renal fibrosis, a hallmark of advanced DKD, results from complex interactions among tubular epithelial injury, interstitial fibroblast activation, excessive extracellular matrix (ECM) deposition, and dysregulated epithelial-stromal crosstalk [7]. Multiple signaling pathways drive these pathologic processes, including transforming growth factor-beta (TGF-β)/Smad, signal transducer and activator of transcription (STAT), Wnt/β-catenin, and chemokine-mediated intercellular communication [8-10]. Recent advances in single-cell and single-nucleus RNA sequencing (scRNA-seq and snRNA-seq) have uncovered considerable heterogeneity among renal cell types and their communication networks, providing new insight into cell-type-specific mechanisms underlying DKD pathogenesis [11, 12].

Traditional Chinese Medicine (TCM) has long been used as an adjunctive therapy for CKD in East Asia [13]. *Abelmoschus manihot (L.) Medik*. (AM), known as Huangkui in TCM and officially documented in the Chinese Pharmacopoeia, has shown significant clinical efficacy in treating DKD [14]. Meta-analyses of randomized controlled trials indicate that AM-containing formulations, when combined with standard care, can improve proteinuria and renal function [15-17]. Preclinical studies further suggest that flavonoids isolated from AM, such as hyperoside and isoquercetin, alleviate oxidative stress, inflammation, and TGF-β1 expression in kidney injury models [18]. Spondin 1 (SPON1), an ECM glycoprotein involved in cell adhesion and tissue remodeling, has been shown to modulate inflammation and fibrosis in extra-renal tissues [19, 20]. However, two key knowledge gaps remain: (1) the cell-specific targets and intercellular communication mechanisms underlying the anti-fibrotic effects of AM in DKD are not well defined, and (2) whether AM influences specific extracellular matrix-associated regulators, particularly SPON1, and its mechanistic role in tissue remodeling and TGF-β signaling, is still unknown.

In this study, we combined a DKD mouse model, snRNA-seq, and targeted *in vitro* validation in high glucose (HG)-treated human renal proximal tubular epithelial (HK-2) cells to characterize the renal response to AM extract. Our aims were to (1) map AM-responsive renal cell populations and transcriptional programs at single-cell resolution, (2) identify ligand-receptor signaling pathways potentially involved in fibrosis-related epithelial-stromal communication, and (3) evaluate whether SPON1 expression changes are associated with the anti-fibrotic effects of AM. By integrating *in vivo* phenotyping, snRNA-seq, and *in vitro* validation, this study provides cell-type-resolved mechanistic clues for the renoprotective effects of AM in DKD and nominates SPON1 as a candidate therapeutic target for diabetic kidney fibrosis.

Materials and methods

Reagents and antibodies

Huangkui capsules, a preparation of AM extract, were provided by Suzhong Pharmaceutical Group Co., Ltd. (Taizhou, China). Each capsule contains 0.43 g of the AM extract. For this study, the AM extract was dissolved in phosphate-buffered saline (PBS) and stored at 4°C. Streptozotocin (STZ; Cat# S0130) and pirfenidone (PFD; Cat# P2116) were purchased from Sigma-Aldrich (USA). STZ was dissolved in 0.1 M sodium citrate buffer (pH 4.5) immediately before use. The following primary antibodies were used: anti-Fibronectin (FN) (Cat# ab-268020; Abcam), anti-TGF-β1 (Cat# 21898-1-AP; Proteintech), anti-SPON1 (Cat# PA5-116176; Thermo Fisher Scientific), and anti-heat shock protein 90 (HSP90) (Cat# 4874; Cell Signaling Technology). Horseradish peroxidase (HRP)-conjugated secondary antibodies against mouse (Cat# GB23301; Servicebio) and rabbit (Cat# GB23303; Servicebio) were used for detection.

Animals and experimental design

All animal procedures were approved by the Animal Research Ethics Committee of Shanghai Sixth People's Hospital (approval no. 2020-022). Six-week-old male C57BL/6J mice (18-22 g) were purchased from Gempharmatech Co., Ltd. (Jiangsu, China) and maintained under specific pathogen-free conditions with a 12 h light/dark cycle, temperature of 22 ± 2°C, and humidity of 50 ± 10%, with free access to food and water. After two weeks of acclimation, mice were randomly divided into three groups (n = 8 per group): the Control group (CON) received a standard chow diet (13.5% kcal from fat, Shanghai Slac Laboratory Animal Co., Ltd.); the DKD group was fed a high-fat diet (HFD, D12492, Research Diets, USA; 60% kcal from

fat, 20% kcal from carbohydrate, 20% kcal from protein) for 8 weeks followed by intraperitoneal injection of STZ (40 mg/kg every other day for three injections). The high-fat diet was continued after STZ injections until the end of the animal experiment to maintain the metabolic phenotype. The AM-treated group (AM) consisted of DKD mice receiving AM extract (2.0 g/kg/day) for 14 weeks [21]. The DKD model was confirmed when random blood glucose levels reached ≥ 16.7 mmol/L and urinary albumin-to-creatinine ratio (UACR) values were ≥ 30 mg/g for two consecutive weeks. All treatments and vehicle were administered daily by oral gavage. Body weight and fasting blood glucose were measured every two weeks. After the treatment period, animals were fasted for 12 h, anesthetized by intraperitoneal injections of 1% pentobarbital sodium (10 μL/g body weight, Cat# P-010, Sigma-Aldrich, USA), and euthanized by cervical dislocation. Death was confirmed by the permanent cessation of circulation and respiration prior to the collection of blood and kidney samples.

Biochemical assays

Urine samples were collected before and after the AM treatment period. Urinary albumin levels were measured using the LBIS Mouse Albumin enzyme-linked immunosorbent assay (ELISA) Kit (Cat# AKRAL-120, FUJIFILM Wako Shibayagi, Japan), and urinary creatinine was quantified using the QuantiChrom Creatinine Assay Kit (Cat# DICT-500, BioAssay Systems, USA). The UACR was calculated by dividing the urinary albumin concentration by the urinary creatinine concentration.

Histologic and immunohistochemical analysis

Kidney tissues were fixed in 10% neutral-buffered formalin, embedded in paraffin, and sectioned at a thickness of 5 μm. Tissue sections were stained with hematoxylin (Cat# H3136, Sigma-Aldrich, USA) and eosin Y (Cat# E4009, Sigma-Aldrich, USA) (H&E), or Masson's trichrome (Cat# G1340, Solarbio, China), to evaluate renal morphology and fibrosis. For immunohistochemistry (IHC), sections were blocked with 10% goat serum for 1 hour at room temperature, then incubated overnight at 4°C with the following primary antibodies: TGF-β1 (1:200), FN (1:500), and SPON1 (1:200). Following primary antibody incubation, sections were treated with appropriate HRP-conjugated secondary antibodies for 1 hour at room temperature. Signal development was performed using diaminobenzidine (DAB), and sections were counterstained with hematoxylin. All stained sections were imaged using an Olympus light microscope.

snRNA-seq

Nuclei isolation was performed using a Nuclei Isolation Kit (Shanghai Biotechnology Corporation, 52009-10). Following the manufacturer's protocol, frozen kidney tissue samples were rapidly added to lysis solution, homogenized, lysed, filtered, centrifuged, and resuspended. The nuclear suspension was stained with trypan blue for counting and microscopic examination, and the concentration was adjusted accordingly. The Chromium Chip G was loaded with nuclear suspension, 10X Barcode Gel Beads, and partitioning oil to create GEMs using the 10X Genomics Chromium platform. GEMs were transferred to a PCR instrument for reverse transcription. Barcoded cDNA was obtained following the system's standard procedure, then purified, amplified, and quantified. After quality control, libraries underwent cluster generation and hybridization with the first sequencing primer before being loaded onto the flow cell for sequencing. Cell type annotation was performed using both the SingleR software (version v1.0.0) and established marker genes. SingleR identifies highly variable genes from reference databases and calculates correlation coefficients between query cells and reference cell types. Through iterative elimination of the least correlated cell types, SingleR ultimately assigns cell type annotations. Differential expression analysis was conducted to identify DEGs between the AM and DKD groups, using a significance threshold of P-value < 0.05 and $|\text{Log}_2\text{FC}| > 1$.

Functional enrichment analyses

To investigate the systemic effect of AM treatment in DKD mice, we performed Gene Set Variation Analysis (GSVA) using hallmark gene sets obtained from the Molecular Signatures Database (MSigDB, Broad Institute). The analysis was conducted on gene expression profiles comparing the DKD group versus the CON group and the AM-treated group versus the DKD group. This approach aimed to identify biological functions and pathways commonly

associated with the observed transcriptional changes. Hallmark gene sets with a normalized enrichment score (NES) absolute value greater than 1 (|NES| > 1) and a false discovery rate (FDR) below 0.05 were considered significant.

Cell-cell communication and trajectory analysis

Cell-cell communication networks were inferred using CellChat (v0.5.0), which predicts ligand-receptor interactions from snRNA-seq data across defined cell clusters. The tool quantified communication probabilities and visualized signaling patterns at both the pathway and cell-type levels. To independently validate and annotate these interactions, inferred ligand-receptor pairs were cross-referenced using iTALK (v0.1.0), which categorizes interactions into four functional classes: cytokines, growth factors, immune checkpoints, and others. Cellular differentiation trajectories were reconstructed using Monocle 2, which orders cells along a pseudotemporal axis based on transcriptional similarity in an unsupervised framework. This reconstruction enabled the inference of lineage progression and state transition dynamics within specific cell populations.

Cell culture and treatment

Human renal proximal tubular epithelial cells (HK-2) were cultured in Dulbecco's Modified Eagle Medium (DMEM)/Low Glucose medium (Cat# E600008-0500, Sangon) supplemented with 10% fetal bovine serum (Cat# E600001, Sangon) and 1% penicillin-streptomycin (Cat# C0222, Beyotime) at 37°C in a 5% CO_2 atmosphere. At 70-80% confluence, cells were subjected to high glucose (HG) stimulation by culturing in medium containing 30 mM glucose for 48 hours; cells maintained in 5 mM glucose (low glucose, LG) served as the control. To evaluate the effects of AM, cells were assigned to the following treatment groups: LG (5 mM glucose); HG (30 mM glucose for 48 h); HG + AM (HG exposure followed by 10 mg/mL AM extract for 24 h); and HG + PFD (HG exposure followed by 200 μg/mL pirfenidone for 24 h).

Immunofluorescence and TUNEL assay

Following treatment, HK-2 cells grown on glass coverslips were fixed with 4% paraformaldehyde for 30 minutes, permeabilized with 0.3% Triton X-100 for 15 minutes, and blocked with 1% bovine serum albumin (BSA) for 1 hour. Cells were then incubated with an anti-SPON1 primary antibody (1:200 dilution) and MitoTracker Red, followed by counterstaining with 4',6-diamidino-2-phenylindole (DAPI) to visualize nuclei. Apoptotic cells were detected using a one-step terminal deoxynucleotidyl transferase dUTP nick end labeling (TUNEL) assay kit (Beyotime, China). All fluorescence images were captured using a confocal laser scanning microscope (Olympus, Japan).

ELISA

The concentrations of TGF-β1 and SPON1 in HK-2 cell culture supernatants were measured using commercial ELISA kits according to the manufacturers' protocols. The TGF-β1 kit (Cat# EL10029) was obtained from Anogen (Canada), and the SPON1 kit (Cat# ELH-FSPON) was from RayBiotech (USA).

Western blotting

HK-2 cells were lysed using radioimmunoprecipitation assay (RIPA) buffer. Total protein concentration was quantified with a bicinchoninic acid (BCA) assay kit, and equal amounts of protein were loaded into wells of 10% sodium dodecyl sulfate-polyacrylamide gel electrophoresis (SDS-PAGE) gels for electrophoretic separation. Subsequently, proteins were transferred onto polyvinylidene difluoride (PVDF) membranes by electroblotting. The membranes were blocked with 5% non-fat milk and then incubated overnight at 4°C with the following primary antibodies: TGF-β1 (1:1000), FN (1:1000), SPON1 (1:1000), and HSP90 (1:1000). After washing, the membranes were incubated with a secondary antibody for 1 hour at room temperature. Protein bands were visualized using a charge-coupled device (CCD) camera-based imaging system (ChemiDoc MP, Bio-Rad, USA), and band intensities were quantified with ImageJ software (version 1.53, National Institutes of Health [NIH], USA).

Quantitative real-time PCR (qRT-PCR)

Total RNA was extracted from kidney tissues and HK-2 cells using TRIzol reagent and reverse-transcribed into cDNA with the PrimeScript™ RT Master Mix (Cat# R433-01, Vazyme) according to the manufacturer's instructions. Quantitative PCR was performed using SYBR Premix Ex Taq™ (Cat# Q312-02, Vazyme) on a

Table 1. Primers used for quantitative real-time polymerase chain reaction (qRT-PCR)

Gene	Species	Forward primer (5'→3')	Reverse primer (5'→3')
COL1A1	Mouse	GTAACAAGGGTGAGCCTGGC	AGCTCCAGAAGGACCTCGAC
COL3A1	Mouse	GGCAGGGACAACTGATGGTG	ACTTAACCCTACGTCGGTGG
COL4A1	Mouse	GAGAGAAAGGTGCTGTGGGC	CGAAGGTCCTGAGTTTCCCG
FN	Mouse	GCAGTGACCACCATTCCTG	GGTAGCCAGTGAGCTGAACAC
TGF-β1	Mouse	TGATACGCCTGAGTGGCTGTCT	CACAAGAGCAGTGAGCGCTGAA
CTGF	Mouse	GGGCCTCTTCTGCGATTTC	ATCCAGGCAAGTGCATTGGTA
PAI-1	Mouse	TTCAGCCCTTGCTTGCCTC	ACACTTTTACTCCGAAGTCGGT
18S	Mouse	AGCTATCAATCTGTCAATCCTGTC	GCTTAATTTGACTCAACACGGGA
TGF-β1	Human	TACCTGAACCCGTGTTGCTCTC	GTTGCTGAGGTATCGCCAGGAA
COL1A1	Human	CCCGAGGCTCTGAAGGTC	GAGCACCATTGGCACCTTT
COL3A1	Human	TGGTCTGCAAGGAATGCCTGGA	TCTTTCCCTGGGACACCATCAG
FN	Human	ACAACACCGAGGTGACTGAGAC	GGACACAACGATGCTTCCTGAG
β-actin	Human	CCTGGCACCCAGCACAAT	ATACTGCTCAGGCCGGG

Note: qRT-PCR, quantitative real-time polymerase chain reaction; COL1A1, collagen type I alpha 1 chain; COL3A1, collagen type III alpha 1 chain; COL4A1, collagen type IV alpha 1 chain; FN, fibronectin; TGF-β1, transforming growth factor-beta 1; CTGF, connective tissue growth factor; PAI-1, plasminogen activator inhibitor-1.

LightCycler 480 system (Roche Diagnostics). Relative gene expression levels were calculated using the 2^(-ΔΔCt) method, with 18S rRNA or β-actin serving as the endogenous control. All primer sequences used in this study are provided in **Table 1**.

Data and statistical analysis

All data are presented as mean ± standard error of the mean (SEM). Statistical significance for animal and cellular experiments was determined by one-way analysis of variance (ANOVA) followed by Tukey's post-hoc test for multiple comparisons. Significance levels are denoted in figures as follows: *P < 0.05, **P < 0.01, #P < 0.05, ##P < 0.01. Western blot and morphologic images shown are representative of at least three independent experiments with consistent results. A *p*-value < 0.05 was considered significant. All statistical analyses and graph generation were performed using GraphPad Prism version 9.0 (GraphPad Software, USA).

Results

AM ameliorates kidney fibrosis in DKD mice and HG injured HK-2 cells

DKD mice exhibited significantly higher fasting blood glucose levels compared to control (CON) mice. AM treatment did not significantly alter blood glucose levels (**Figure 1A**). Renal function, assessed by the UACR, was markedly elevated in DKD mice, and this increase was significantly attenuated by AM treatment (**Figure 1B**). Although body weight did not differ significantly between the AM-treated and DKD groups, the DKD group showed a notable increase in body weight relative to the CON group (**Figure 1C**). Kidney tissues were analyzed by H&E staining, Masson's trichrome staining, and immunohistochemistry for TGF-β1 and FN (**Figure 1E**). Compared to CON mice, DKD mice exhibited mesangial cell proliferation, tubular atrophy, collagen accumulation, and interstitial fibrosis. These pathologic signs were ameliorated following AM treatment. Consistent with the histological results, qRT-PCR analysis demonstrated that AM treatment reduced the elevated mRNA levels of fibrosis-related genes, COL1A1, COL3A1, COL4A1, FN, PAI-1, CTGF, and TGF-β1, in the kidneys of DKD mice (**Figure 1D**). In HG injured HK-2 cells, the concentration of TGF-β1 in the culture supernatant was increased under HG conditions, and this effect was counteracted by both AM and PFD treatment (**Figure 1F**). Similarly, mRNA levels of fibrosis markers (TGF-β1, COL1A1, COL3A1, FN) were elevated by HG exposure, and both AM and PFD treatment effectively reduced these levels (**Figure 1G**). Western blot analysis further confirmed these findings (**Figure 1H**).

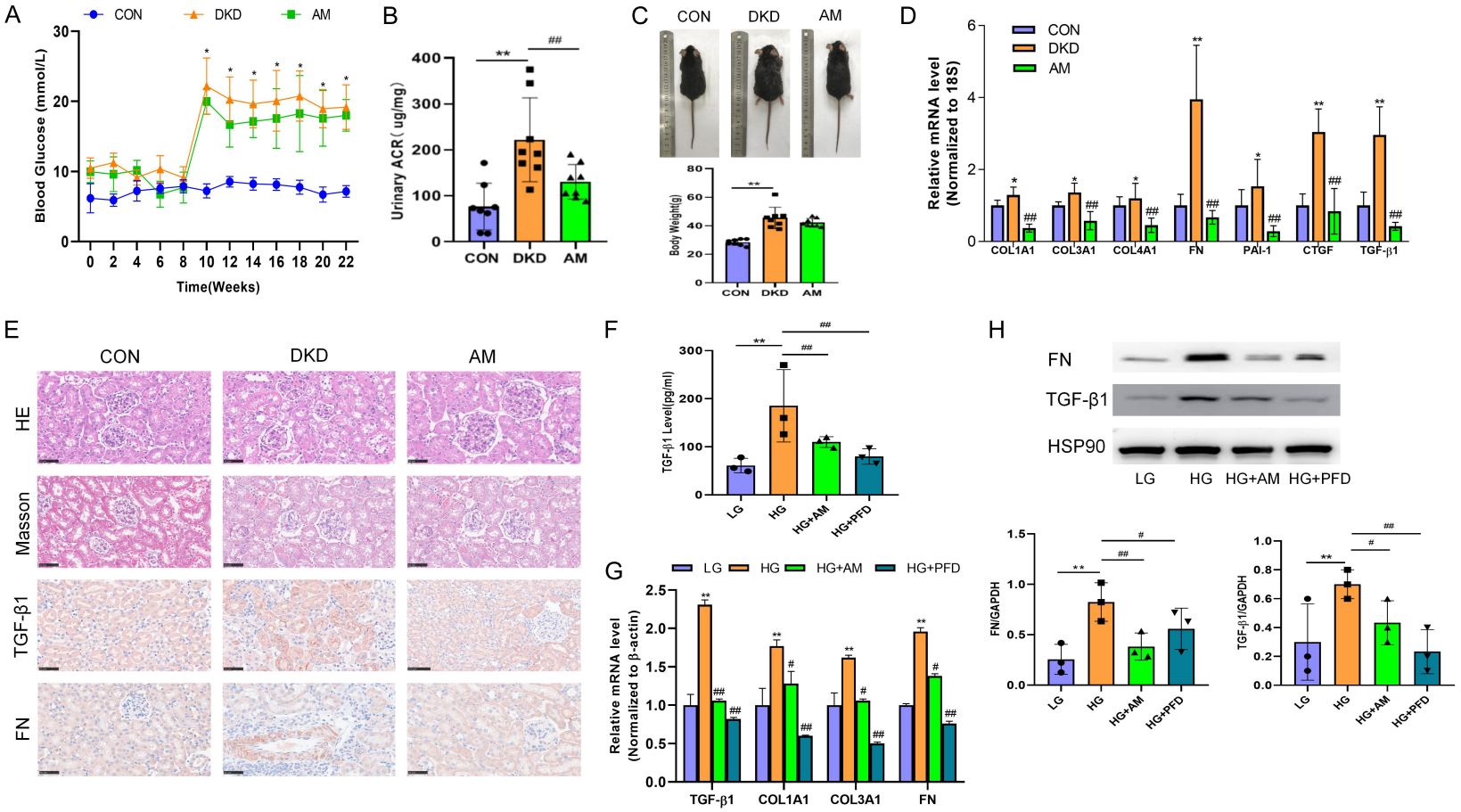

Figure 1. AM ameliorates renal fibrosis in high-fat diet (HFD)/streptozotocin (STZ)-induced diabetic mice and high glucose (HG)-injured human renal proximal tubular epithelial (HK-2) cells. A. Blood glucose levels across experimental groups. B. Urinary albumin-to-creatinine ratios (ACRs). C. Representative photographs of mice and quantification of body weight across experimental groups (n = 8). D. mRNA expression of fibrosis-related genes in kidney tissues measured by quantitative real-time polymerase chain reaction (qRT-PCR) (n = 8). E. Kidney sections stained with hematoxylin and eosin (H&E) and Masson's trichrome showing mesangial expansion and fibrosis in diabetic mice. Immunohistochemistry for transforming growth factor-beta 1 (TGF-β1) and fibronectin (FN) illustrates amelioration of renal fibrosis following Abelmoschus manihot (AM) treatment. Scale bar = 50 μm. F. TGF-β1 concentration in cell culture supernatant of HK-2 cells measured by enzyme-linked immunosorbent assay (ELISA) (n = 3). G. mRNA expression of fibrosis markers in HK-2 cells assessed by qRT-PCR (n = 3). H. Immunoblot analysis of TGF-β1 and FN protein levels in HG-stimulated HK-2 cells (n = 3). All data are presented as mean ± standard error of the mean (SEM). For animal experiments, *P < 0.05, **P < 0.01 versus control (CON) group; #P < 0.05, ##P < 0.01 versus diabetic kidney disease (DKD) group. For cellular experiments, *P < 0.05, **P < 0.01 versus low glucose (LG) group; #P < 0.05, ##P < 0.01 versus HG group.

snRNA-seq identified cell populations responsive to AM

Following data preprocessing and quality control, a total of 51,874 single nuclei from the CON, DKD, and AM groups were profiled (**Figure 2A**). The number of detected genes per cell increased in nearly all cell populations in the DKD group and decreased following AM treatment (**Figure 2B**). Unsupervised clustering identified 11 distinct clusters, which were annotated as specific cell types based on established marker genes from previous kidney and glomerular single-cell datasets (**Figure 2C**). Endothelial cell (EC) subtypes expressed characteristic markers including *Ptprb*, *Emcn*, and *Pecam1*. Mesangial (Mesan) cells, defined by expression of *Slit3*, *Itga8*, and *Pdgfrb*, were clearly distinguished from interstitial cells (Int). The Int population included vascular smooth muscle cells marked by *Tagln*. Proximal tubule (PT) segments were identified as PT-S1, PT-S2, and PT-S3 based on segment-specific marker expression: S1 (*Slc5a2*, *Slc22a8*, *Gatm*), S2 (*Slc13a3*, *Slc13a1*), and S3 (*Slc7a13*, *Atp1la*). Comparative transcriptome analysis identified 5,506 differentially expressed genes (DEGs) between DKD and CON groups, and 4,354 DEGs between AM and DKD groups, across all cell types. Int and PT cells showed the highest numbers of DEGs in response to AM treatment (**Figure 2D**), indicating these cell types as the primary responders to AM in the DKD context.

AM suppressed profibrotic signaling in Int and PT-S1 subsets

To assess the effect of AM treatment on the renal fibrotic microenvironment, we analyzed the cellular proportions of PT-S1 and Int subsets. DKD mice exhibited a decreased proportion of PT-S1 cells and an increased proportion of Int cells compared to controls. Although the differences between the AM and DKD groups did not reach statistical significance, AM treatment was associated with a trend toward increased PT-S1 cells and decreased Int cells (**Figure 3A**). We next examined the expression of fibrosis-related markers across groups. A bubble plot visualization showed elevated expression of *TGFβ1*, *Col3A1*, *Col1A1*, *SMAD family member 3 (SMAD3)*, *STAT3*, and *STAT6* in DKD mice, which was reduced following AM treatment (**Figure 3B**), further confirming the anti-fibrotic effect of AM in DKD. Analysis of differentially expressed genes (DEGs) revealed that in the Int cluster, genes including *Wbscr17*, *Sntg1*, *Cdk14*, *Pdzrn3*, and *Spon1* were upregulated in DKD and downregulated after AM treatment (**Figure 3C**). Similarly, in the PT-S1 cluster, genes such as *Large*, *Rbpms*, *Zmiz1*, *Dock1*, and *Col4a2* showed increased expression in DKD that was reversed by AM (**Figure 3D**). We further investigated transcriptomic changes in PT-S1 cells using Gene Set Variation Analysis (GSVA) with Hallmark gene sets. This analysis identified TGF-β signaling and apoptosis as the most significantly enriched pathways in DKD mice. AM treatment specifically downregulated TGF-β signaling activity (**Figure 3E**, **3F**), suggesting that its anti-fibrotic effect is mediated, at least in part, through suppression of TGF-β-driven profibrotic processes in PT-S1 cells.

Pseudotime analysis reveals stage-specific modulation

To further investigate the cell type-specific mechanisms underlying the therapeutic effects of AM, we performed cell trajectory analysis using the Monocle 2 package (**Figure 4A**). The density distribution of cells from CON, DKD, and AM groups across pseudotime is shown in **Figure 4B**. AM influenced PT cells predominantly at later pseudotime stages, while affecting EC, Mesan, podocyte (Podo), and Int cells at earlier stages (**Figure 4C**). During the transition process, the relative expression levels of *SMAD3*, *TGFβ1*, and *SPON1* exhibited similar trajectory patterns across all groups (**Figure 4D-F**).

AM remodeled ligand-receptor communication networks in DKD kidneys

We used CellChat to analyze intercellular interactions among different cell types. Analysis revealed PT-S2 cells interacting with PT-S3 cells by colony-stimulating factor (CSF) signaling, while Int cells communicated with PT-S3 cells through C-X-C motif chemokine ligand (CXCL) signaling (**Figure 5A**, **5B**). Overall interaction strength increased between PT-S1 and Int cells in the DKD condition (**Figure 5C**). Using iTALK and its built-in receptor-ligand pair database, we further identified signaling events among Int, PT-S1, PT-S2, and PT-S3 cells. Among the cytokine-receptor pairs analyzed, PT-S1 displayed the largest number of differentially upregulated communication pairs with other cell types (**Figure 5D**).

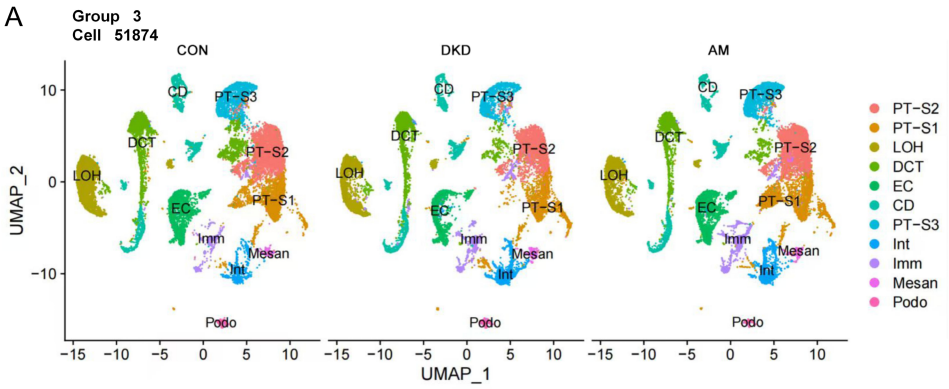

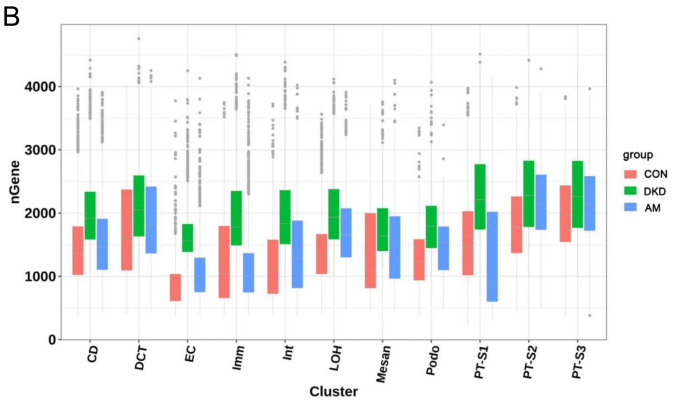

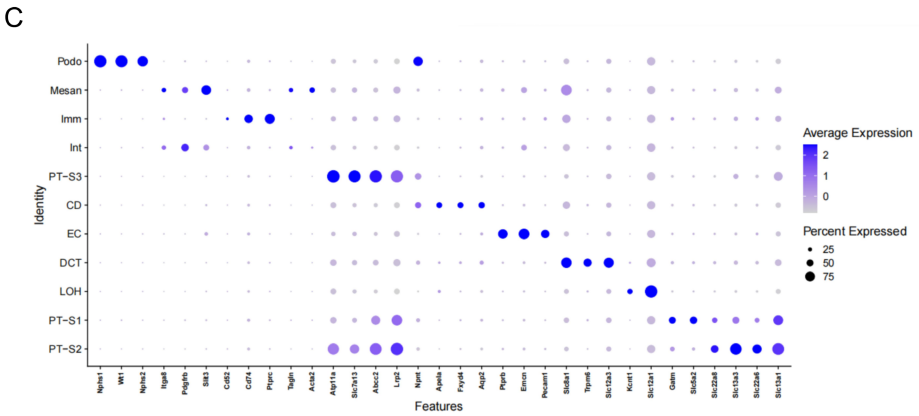

D

nDEG:	DKD vs.CON		AM vs.DKD	
	Up	Down	Up	Down
Mesan	382	129	388	862
Podo	375	472	177	464
Int	469	537	95	136
EC	501	25	82	121
Imm	478	507	39	420
DCT	144	167	112	34
LOH	185	18	74	28
CD	125	45	99	45
PT-1	518	21	47	786
PT-2	137	164	69	131
PT-3	80	27	80	65
Total	**3394**	**2112**	**1262**	**3092**

Figure 2. Single-nucleus RNA sequencing (snRNA-seq) analysis of kidneys from high-fat diet (HFD)/streptozotocin (STZ)-induced diabetic mice treated with Abelmoschus manihot (AM). A. Uniform Manifold Approximation and Projection (UMAP) visualization of 11 annotated cell types across experimental groups. B. Alterations in the number of detected genes (nGene) per cell cluster among groups. C. Dot plot displaying defining marker genes for each annotated cell type. D. Total number of significant differentially expressed genes (DEGs) identified per cell type.

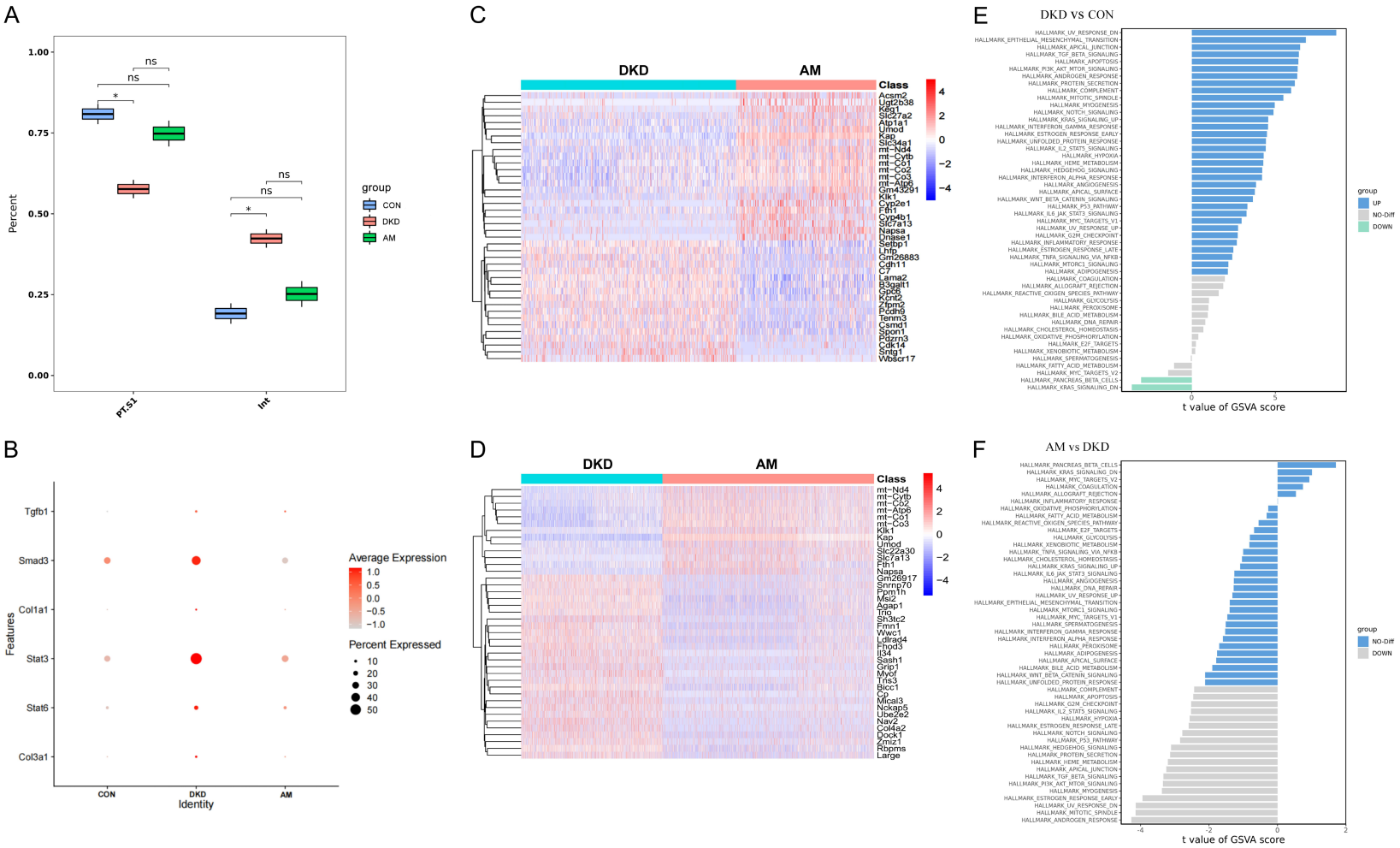

Figure 3. Gene expression and pathway alterations in proximal tubular segment 1 (PT-S1) and interstitial (Int) cells in response to Abelmoschus manihot (AM) treatment. A. Proportion of PT-S1 and Int cells across control (CON), diabetic kidney disease (DKD), and AM groups presented as box plots. The central line indicates the median; lower and upper bounds represent the 25th and 75th percentiles, respectively. B. Dot plot visualization of fibrosis-related gene expression across groups. C. Heatmap of differentially expressed genes (DEGs) between DKD and AM groups within Int cells. D. Heatmap of DEGs between DKD and AM groups within PT-S1 cells. E. Hallmark pathway enrichment comparison between DKD and CON groups in PT-S1 cells based on Gene Set Variation Analysis (GSVA). F. Hallmark pathway enrichment comparison between AM and DKD groups in PT-S1 cells based on GSVA. *P < 0.05; ns, not significant.

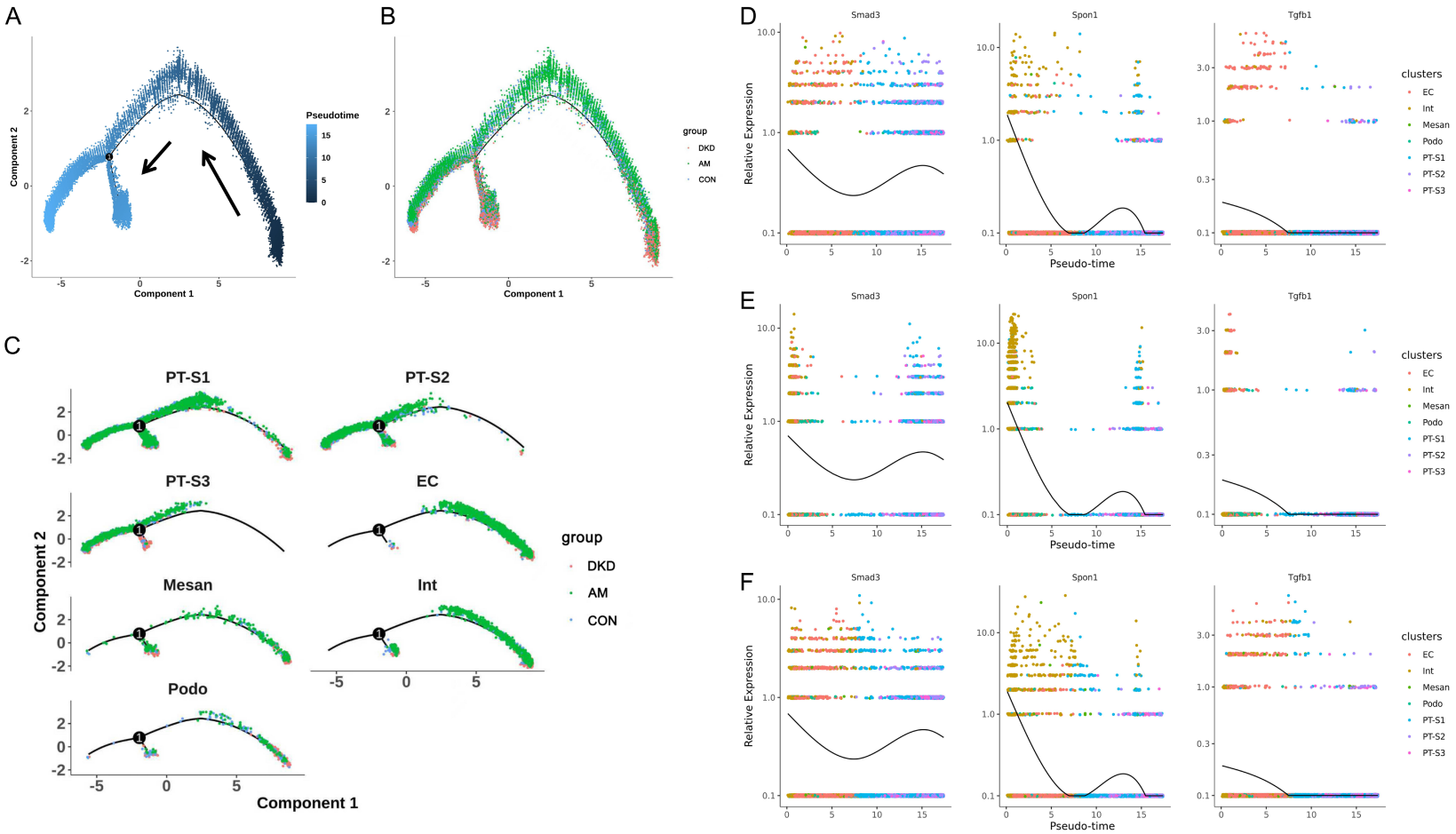

Figure 4. Cellular trajectory analysis inferred by Monocle 2. (A) Pseudotime trajectory of all cell clusters. (B) Pseudotime trajectory distribution across experimental groups. (C) Pseudotime trajectories illustrating cluster differentiation in control (CON), diabetic kidney disease (DKD), and Abelmoschus manihot (AM) groups. (D-F) Expression trends of transforming growth factor-beta 1 (TGF-β1), SMAD family member 3 (SMAD3), and spondin 1 (SPON1) along pseudotime in CON (D), DKD (E), and AM (F) groups. EC, endothelial cell; Int, interstitial; Mesan, mesangial; Podo, podocyte; PT-S1/S2/S3, proximal tubular segment 1/2/3.

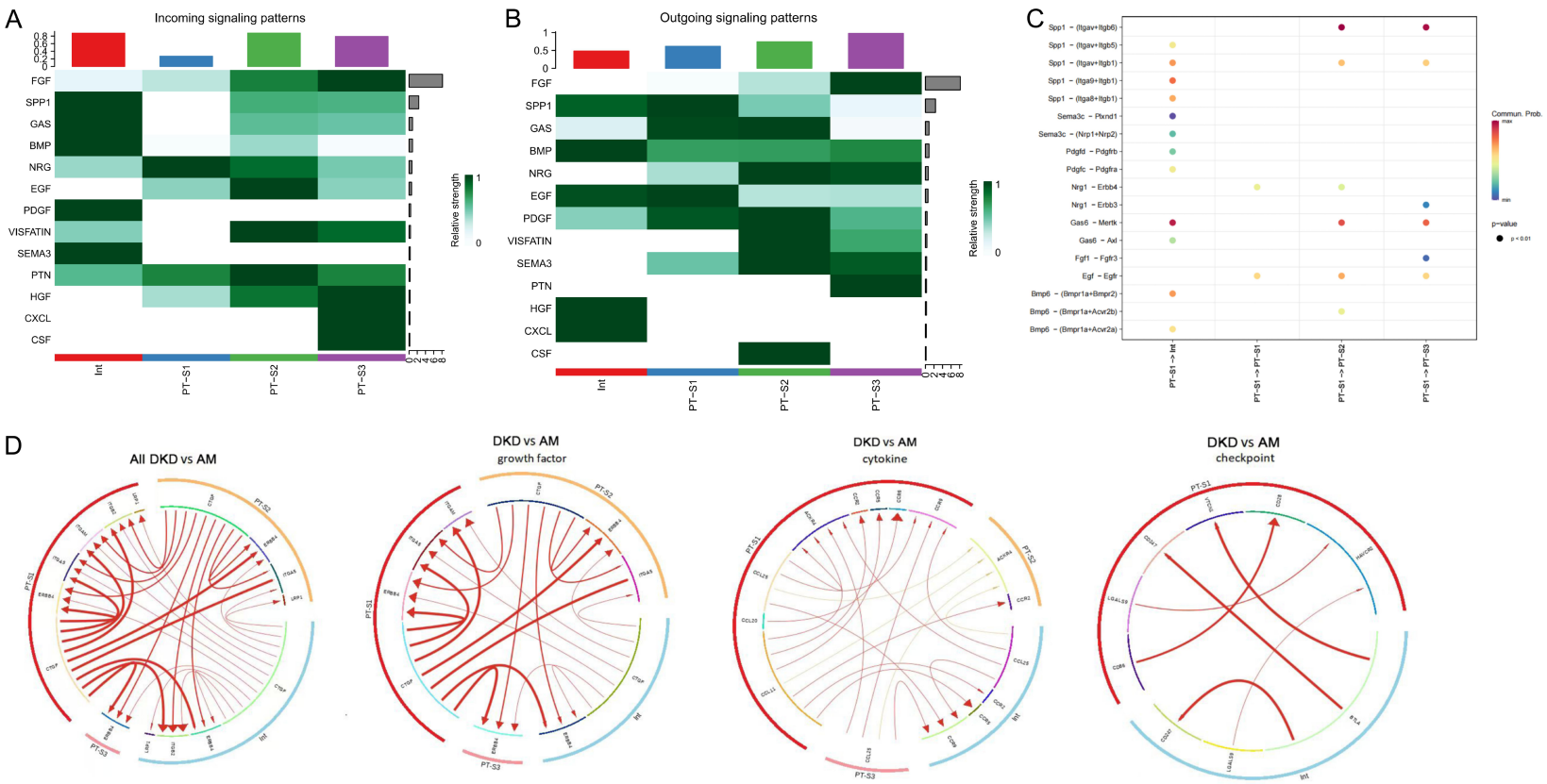

Figure 5. Ligand-receptor interactions modulated by *Abelmoschus manihot* (AM) treatment. A, B. Heatmaps of dominant incoming and outgoing signaling pathway patterns across diverse cell clusters. C. Dot plot summarizing interaction strengths and signaling probabilities among interstitial (Int), proximal tubular segment 1 (PT-S1), segment 2 (PT-S2), and segment 3 (PT-S3) cells. The size of the dots represents the *P*-value significance ($P < 0.01$), and the color scale indicates the communication probability. D. Chord diagrams illustrating enriched ligand-receptor interactions categorized by functional classes (growth factor, cytokine, and checkpoint) across major cell types in AM-treated versus diabetic kidney disease (DKD) kidneys.

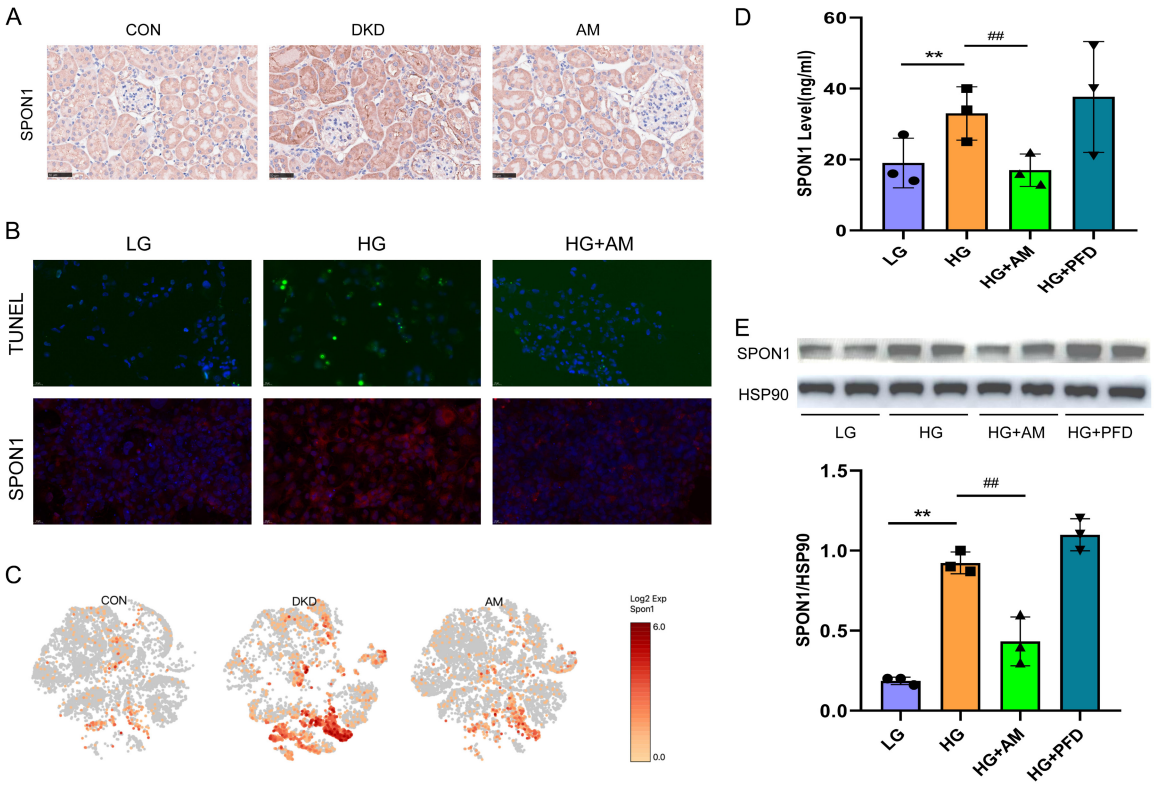

Figure 6. *Abelmoschus manihot* (AM) reduces spondin 1 (SPON1) expression in diabetic kidney disease (DKD) mice and high glucose (HG)-induced human renal proximal tubular epithelial (HK-2) cells. A. Immunohistochemistry (IHC) showing elevated SPON1 in DKD kidney tissues and its reduction after AM treatment. Scale bar = 50 μm. B. Representative fluorescence images of terminal deoxynucleotidyl transferase dUTP nick end labeling (TUNEL) assay (green) and SPON1 staining (red) in kidneys. Scale bar = 20 μm. C. t-distributed stochastic neighbor embedding (t-SNE) visualization of SPON1 expression across various cell types. D. SPON1 concentration in the culture supernatant of HK-2 cells measured by enzyme-linked immunosorbent assay (ELISA). E. Western blot analysis and quantification of SPON1 and heat shock protein 90 (HSP90) in HG-stimulated HK-2 cells. Data represent mean ± standard error of the mean (SEM); **P < 0.01 versus low glucose (LG) group; ##P < 0.01 versus HG group; n = 3.

AM reduced SPON1 expression and apoptosis in DKD mice and HK-2 cells

To evaluate the effect of AM on SPON1 expression *in vivo* and *in vitro*, HK-2 cells were exposed to high glucose (30 mM) prior to AM treatment. Immunohistochemical staining showed increased SPON1 expression in DKD mice, which was reduced following AM treatment (**Figure 6A**). Confocal microscopy revealed enhanced terminal deoxynucleotidyl transferase dUTP nick end labeling (TUNEL) and SPON1 fluorescence intensity in DKD mice, both of which were decreased by AM treatment (**Figure 6B**). snRNA-seq data indicated high expression of *SPON1* in Int cells (**Figure 6C**). In HK-2 cells, AM reduced the secretion of SPON1 into the supernatant (**Figure 6D**). Western blot analysis confirmed these findings (**Figure 6E**). Collectively, these results demonstrate that AM suppresses SPON1 expression in both DKD mice and HG-induced HK-2 cells.

Discussion

In the present study, we combined *in vivo* phenotyping, histopathology, snRNA-seq, and targeted *in vitro* validation to investigate the anti-fibrotic effects of AM in DKD. Our data show that AM attenuated renal fibrosis and was associated with cell-type-specific transcriptional remodeling, particularly in proximal tubular and interstitial compartments, as well as altered epithelial-stromal ligand-receptor communication. Among the AM-responsive fibrosis-related genes, SPON1 emerged as a consistently regulated candidate across transcriptomic and validation datasets. Although

these findings link AM treatment to reduced SPON1 expression and attenuation of profibrotic signaling, direct causal mediation by SPON1 remains to be established in future gain-/loss-of-function and rescue studies.

Clinical meta-analyses have indicated that AM, commonly administered as Huangkui capsules in combination with RAS inhibitors, significantly reduces proteinuria and improves renal function in DKD patients [22]. Additional studies have reported that AM treatment can reduce blood urea nitrogen (BUN), serum creatinine, and 24-hour urine protein levels, while improving GFR and serum albumin levels [23]. Our findings provide mechanistic support for these clinical observations at the cellular level, thereby helping to bridge the translational gap between clinical efficacy and molecular mechanisms of AM in DKD treatment.

Previous mechanistic studies on AM have focused primarily on its ability to inhibit oxidative stress [24], podocyte injury [25], inflammatory responses [26], TGF-β1/Smad signaling [27], and mesangial cell proliferation [28], while also demonstrating its role in enhancing immune function [29], protecting renal tubular epithelial cells [30], and ameliorating renal fibrosis [31] in DKD models. For example, total flavones of AM were found to ameliorate podocyte necroptosis by suppressing the receptor-interacting serine/threonine-protein kinase 1 (RIPK1)/RIPK3/mixed lineage kinase domain-like protein (MLKL) axis in a DKD rat model [32]. Another study showed that AM combined with finerenone attenuated DKD progression by inhibiting the Janus kinase 2 (JAK2)/signal transducer and activator of transcription 3 (STAT3) pathway, thereby reducing inflammation, apoptosis, and tubular injury [33]. Work from our team has also indicated that AM ameliorates renal tubulopathy in DKD and promotes mitophagy partly through upregulation of the stimulator of interferon genes 1 (STING1)/PTEN-induced kinase 1 (PINK1) pathway [21]. Additional research demonstrated that AM attenuates tubulointerstitial injury and renal interstitial fibrosis in a unilateral ureteral obstruction mouse model [34]. Collectively, these findings establish a strong therapeutic rationale for AM in treating DKD and other renal diseases. Our current study extends this mechanistic understanding by identifying cell type-specific responses to AM through snRNA-seq analysis and by revealing SPON1, a matricellular protein previously understudied in renal fibrosis, as a key mediator of its anti-fibrotic effects.

Multiple lines of evidence from this study indicate that AM exerts its anti-fibrotic effects through coordinated suppression of epithelial-stromal crosstalk and ECM remodeling. First, snRNA-seq analysis revealed that Int and PT-S1 cell clusters exhibited the highest numbers of DEGs following AM treatment, identifying these compartments as primary therapeutic targets. Second, pseudotime trajectory analysis demonstrated that AM shifted renal cell populations from late-stage fibrogenic states toward earlier, less activated states, thereby attenuating disease progression. Third, ligand-receptor interaction analysis showed that DKD kidneys exhibited enhanced communication through CXCL and CSF pathways between PT-S1 and Int cells, and AM treatment substantially reduced these profibrotic signaling axes. Finally, targeted experimental validation confirmed that SPON1 expression, significantly upregulated in DKD, was suppressed by AM both *in vivo* and *in vitro*, and this reduction correlated with decreased apoptosis and fibrosis.

SPON1 was initially identified as a factor promoting neural cell adhesion and axon guidance in vertebrates [35], with subsequent roles reported in neuronal differentiation [36] and circadian rhythm regulation [37]. It has also been implicated in Alzheimer's disease pathogenesis [38] and serves as a prognostic biomarker in ovarian cancer [39]. Beyond neural and oncological contexts, SPON1 participates in extra-renal fibrotic processes; for example, in idiopathic pulmonary fibrosis, SPON1 circular RNA was shown to regulate TGF-β1/Smad3 signaling and fibroblast activation [40]. Although direct evidence in renal fibrosis has been limited, our findings position SPON1 as a plausible mediator linking tubular and interstitial remodeling with ECM deposition in DKD. As an extracellular matrix-associated protein, the exact molecular mechanism by which AM downregulates SPON1 warrants further investigation. Based on our GSVA results, which demonstrated a significant downregulation of TGF-β pathway activity following AM treatment, we speculate that AM may indirectly reduce SPON1

expression by blunting upstream TGF-β/Smad-mediated transcriptional activation. This links the suppression of upstream profibrotic signaling with downstream ECM remodeling, constructing a more complete mechanistic model for the anti-fibrotic effects of AM.

The strengths of this study include the integration of snRNA-seq profiling with functional validation, which provided a high-resolution view of renal cell-type-specific responses to AM. Furthermore, the combination of *in vivo* and *in vitro* approaches established the mechanistic relevance of SPON1 in the context of DKD. However, several limitations should be considered. First, although SPON1 was consistently associated with AM treatment and fibrosis-related changes across snRNA-seq and *in vitro* validation, direct causal evidence (e.g., gain-/loss-of-function and rescue experiments) is not yet available. Second, while snRNA-seq identified interstitial cells as the predominant source of SPON1, our *in vitro* validation was conducted in HK-2 cells. This choice was based on the fact that proximal tubular epithelial cells (TECs) are primary sensors of high glucose injury and active participants in the fibrotic process. Injured TECs can secrete various matricellular proteins that modulate the interstitial microenvironment through epithelial-mesenchymal crosstalk [41]. The observed upregulation of SPON1 in HG-treated HK-2 cells suggests that tubular cells also contribute to the total SPON1 pool in the DKD kidney. However, we acknowledge that HK-2 cells may not fully represent the primary effector mechanisms in the interstitium. Future studies using fibroblast cell lines, such as NRK-49F, will be instrumental in further dissecting the cell-type-specific contributions of SPON1. Third, while the snRNA-seq analysis provided cell-type-resolved insights into AM-responsive pathways and intercellular communication, additional external validation (including independent datasets and human kidney samples) would further strengthen the translational relevance of these findings. Therefore, our results should be interpreted as providing mechanistic clues and hypothesis-generating evidence rather than definitive proof of SPON1-mediated causality.

Based on these encouraging findings, future studies should aim to evaluate AM or its active flavonoid components in larger, well-controlled human DKD cohorts, correlating changes in SPON1 expression or other ECM-remodeling biomarkers with clinical outcomes. In addition, targeted inhibition or modulation of SPON1, using approaches such as small interfering RNA (siRNA) or neutralizing antibodies in renal fibrosis models, would help clarify its causal role in disease progression. Finally, further exploration of how AM influences intercellular communication networks and the renal microenvironment may reveal additional therapeutic targets and inform optimized combination treatment strategies, for instance with SGLT2 inhibitors or MRAs.

Conclusion

AM extract attenuated renal fibrosis in DKD and was associated with altered epithelial-stromal communication, reduced SPON1 expression, and remodeling of profibrotic ligand-receptor networks. These findings provide cell-type-resolved mechanistic clues for the renoprotective effects of AM and identify SPON1 as a candidate molecular target in diabetic kidney fibrosis. Further functional studies are warranted to determine the causal role of SPON1 in mediating the anti-fibrotic effects of AM.

Acknowledgements

This work was supported by the National leading unit of cooperation between Chinese and Western medicine for major and difficult diseases ZY (2018-2020) FWTX-2003, National Key Clinical Specialty (Z155080000004), and Shanghai Municipal Key Clinical Specialty.

Disclosure of conflict of interest

None.

Abbreviations

CKD, chronic kidney disease; ESRD, end-stage renal disease; DKD, diabetic kidney disease; RAS, renin-angiotensin system; CON, Control; AM, *Abelmoschus manihot (L.)* Medik; UACR, urinary albumin/creatinine ratio; BUN, blood urea nitrogen; COL, Collagen; FN, Fibronectin; CTGF, connective tissue growth factor; PAI-1, plasminogen activator inhibitor-1; SGLT2, sodium glucose cotransporter-2; MRA, mineralocor-

ticoid receptor antagonists; ARB, angiotensin receptor blocker; ACEI, angiotension converting enzyme inhibitors; GFR, glomerular filtration rate; RCT, randomized controlled trial; PFD, Pirfenidone; ECM, extracellular matrix; snRNA-seq, single-nucleus RNA sequencing; GEM, gene expression modulator; DEG, differentially expressed gene; GSVA, gene set variation analysis; PT, proximal tubular; Int, Interstitial; DCT, distal convoluted tubule; EC, endothelial cell; Mesan, Mesangial; Podo, Podocyte; LOH, loop of Henle; Imm, Immune; CD, collecting duct.

Address correspondence to: Jun Yin and Li Wei, Department of Endocrinology and Metabolism, Shanghai Sixth People's Hospital Affiliated to Shanghai Jiao Tong University School of Medicine, 600 Yishan Road, Shanghai 200233, China. E-mail: yinjun@sjtu.edu.cn (JY); weili6th@shsmu.edu.cn (LW)

References

[1] Borhade MB, Yashi K and Singh S. Diabetes and exercise. StatPearls Publishing; 2025.

[2] Alicic RZ, Rooney MT and Tuttle KR. Diabetic kidney disease: challenges, progress, and possibilities. Clin J Am Soc Nephrol 2017; 12: 2032-2045.

[3] Calle P and Hotter G. Macrophage phenotype and fibrosis in diabetic nephropathy. Int J Mol Sci 2020; 21: 2806.

[4] Yan G, Chang T, Zhao Y, Yu M, Mi J, Wang G, Wang X and Liao X. The effects of ophiocordyceps sinensis combined with ACEI/ARB on diabetic kidney disease: a systematic review and meta-analysis. Phytomedicine 2023; 108: 154531.

[5] Cai X, Cao H, Wang M, Yu P, Liang X, Liang H, Xu F and Cai M. SGLT2 inhibitor empagliflozin ameliorates tubulointerstitial fibrosis in DKD by downregulating renal tubular PKM2. Cell Mol Life Sci 2025; 82: 159.

[6] Barrera-Chimal J, Lima-Posada I, Bakris GL and Jaisser F. Mineralocorticoid receptor antagonists in diabetic kidney disease - mechanistic and therapeutic effects. Nat Rev Nephrol 2022; 18: 56-70.

[7] Kuppe C, Ibrahim MM, Kranz J, Zhang X, Ziegler S, Perales-Patón J, Jansen J, Reimer KC, Smith JR, Dobie R, Wilson-Kanamori JR, Halder M, Xu Y, Kabgani N, Kaesler N, Klaus M, Gernhold L, Puelles VG, Huber TB, Boor P, Menzel S, Hoogenboezem RM, Bindels EMJ, Steffens J, Floege J, Schneider RK, Saez-Rodriguez J, Henderson NC and Kramann R. Decoding myofibroblast origins in human kidney fibrosis. Nature 2021; 589: 281-286.

[8] Hong Q, Kim H, Cai GY, Chen XM, He JC and Lee K. Modulation of TGF-β signaling new approaches toward kidney disease and fibrosis therapy. Int J Biol Sci 2025; 21: 1649-1665.

[9] Liu Y, Wang W, Zhang J, Gao S, Xu T and Yin Y. JAK/STAT signaling in diabetic kidney disease. Front Cell Dev Biol 2023; 11: 1233259.

[10] Cohen C, Mhaidly R, Croizer H, Kieffer Y, Leclere R, Vincent-Salomon A, Robley C, Anglicheau D, Rabant M, Sannier A, Timsit MO, Eddy S, Kretzler M, Ju W and Mechta-Grigoriou F. WNT-dependent interaction between inflammatory fibroblasts and FOLR2+ macrophages promotes fibrosis in chronic kidney disease. Nat Commun 2024; 15: 743.

[11] Zhou Y, Fang X, Huang LJ and Wu PW. Transcriptome and single-cell profiling of the mechanism of diabetic kidney disease. World J Diabetes 2025; 16: 101538.

[12] Li L, Tao M, Gao X, Cao Q, Liao Z, Chen F, Yusufu A, Nie H, Zeng Z, Huang K, Deng X, Gao P and Wu X. Uncovering key markers and therapeutic targets for renal fibrosis in diabetic kidney disease through bulk and single-cell RNA sequencing. J Transl Med 2025; 23: 742.

[13] Shen S, Zhong H, Zhou X, Li G, Zhang C, Zhu Y and Yang Y. Advances in Traditional Chinese Medicine research in diabetic kidney disease treatment. Pharm Biol 2024; 62: 222-232.

[14] Saxu R, Tang H, Yu H, Ge H and Gu HF. Huangkui capsule, an extract from Abelmoschus manihot (L.) medic, inhibits adrenal aldosterone synthesis and renal ERK/EGR1 pathway in the treatment of diabetic kidney disease. J Ethnopharmacol 2025; 349: 119936.

[15] An W, Huang Y, Chen S, Teng T, Liu J and Xu Y. Efficacy and safety of Huangkui capsule for diabetic nephropathy: a protocol for systematic review and meta-analysis. Medicine (Baltimore) 2021; 100: e27569.

[16] Shi L, Feng L, Zhang M, Li X, Yang Y, Zhang Y and Ni Q. Abelmoschus manihot for diabetic nephropathy: a systematic review and meta-analysis. Evid Based Complement Alternat Med 2019; 2019: 9679234.

[17] Tan Y, Zhang Z, Zhou P, Zhang Q, Li N, Yan Q, Huang L and Yu J. Efficacy and safety of Abelmoschus manihot capsule combined with ACEI/ARB on diabetic kidney disease: a systematic review and meta analysis. Front Pharmacol 2024; 14: 1288159.

[18] Jash R, Maji HS, Chowdhury A, Biswas S, Maparu K, Khatun R and Dey S. Rutin reduces inflammation and fibrosis via TGF-β/SMAD pathways in IgA nephropathy induced rats. Nephrology (Carlton) 2024; 29: 717-728.

[19] Yang J, Xiang X, Wen S, Yu Z, Ai H, Wang Y, Liang H, Li S, Lu Y, Zhu Y, Shi G and Chen Y. Comprehensive analysis of endoplasmic reticulum-related and secretome gene expression profiles in the progression of non-alcoholic fatty liver disease. Front Endocrinol (Lausanne) 2022; 13: 967016.
[20] Whately KM, Sengottuvel N, Edatt L, Srivastava S, Woods AT, Tsai YS, Porrello A, Zimmerman MP, Chack AC, Jefferys SR, Yacovone G, Kim DJ, Dudley AC, Amelio AL and Pecot CV. Spon1+ inflammatory monocytes promote collagen remodeling and lung cancer metastasis through lipoprotein receptor 8 signaling. JCI Insight 2024; 9: e168792.
[21] Zhu Z, Luan G, Peng S, Fang Y, Fang Q, Shen S, Wu K, Qian S, Jia W, Ye J and Wei L. Huangkui capsule attenuates diabetic kidney disease through the induction of mitophagy mediated by STING1/PINK1 signaling in tubular cells. Phytomedicine 2023; 119: 154975.
[22] Li Y, Wu C, Song C, Liu S and Nan Z. Efficacy and safety of Huangkui capsule for diabetic nephropathy: a systematic review and meta-analysis. Medicine (Baltimore) 2024; 103: e38417.
[23] Wei LI, Ping X, Wei S, Jing Z, Qiong L, Lianyi G, Yao Z and Kun G. Effects of the Huangkui capsule on chronic kidney disease: a systematic review and Meta-analysis. J Tradit Chin Med 2023; 43: 6-13.
[24] Su J, Zhang Y, Wang X, Hu X, Zhou K, Zhu H, Liu E and Liu S. Huangkui capsules regulate tryptophan metabolism to improve diabetic nephropathy through the Keap1/Nrf2/HO-1 pathway. Front Pharmacol 2025; 16: 1535352.
[25] Zhao L, Han S and Chai C. Huangkui capsule alleviates doxorubicin-induced proteinuria via protecting against podocyte damage and inhibiting JAK/STAT signaling. J Ethnopharmacol 2023; 306: 116150.
[26] Qu B, Li G, Zhao N, Li R, Ma H, Zhu H, Li P and Zhao J. Exploring the therapeutic potential of Abelmoschi Corolla in psoriasis: mechanisms of action and inflammatory pathway disruption. Phytomedicine 2025; 138: 156379.
[27] Gu LY, Sun Y, Tang HT and Xu ZX. Huangkui capsule in combination with metformin ameliorates diabetic nephropathy via the Klotho/TGF-β1/p38MAPK signaling pathway. J Ethnopharmacol 2021; 281: 113548.
[28] Wu W, Hu W, Han WB, Liu YL, Tu Y, Yang HM, Fang QJ, Zhou MY, Wan ZY, Tang RM, Tang HT and Wan YG. Inhibition of Akt/mTOR/p70S6K signaling activity with Huangkui capsule alleviates the early glomerular pathological changes in diabetic nephropathy. Front Pharmacol 2018; 9: 443.
[29] Zhang X, Zeng Y, Tang Y, Wang Y, Yang X, Deng Z, Liang L, Yang C, Yan J and He G. Multidimensional immunomodulation by abelmoschi corolla polysaccharide: Gut barrier restoration, microbiota remodelling, and systemic metabolic regulation. Phytomedicine 2025; 149: 157545.
[30] Yu H, Tang H, Wang M, Xu Q, Yu J, Ge H, Qiang L, Tang W and Gu HF. Effects of total flavones of Abelmoschus manihot (L.) on the treatment of diabetic nephropathy via the activation of solute carriers in renal tubular epithelial cells. Biomed Pharmacother 2023; 169: 115899.
[31] Li N, Tang H, Wu L, Ge H, Wang Y, Yu H, Zhang X, Ma J and Gu HF. Chemical constituents, clinical efficacy and molecular mechanisms of the ethanol extract of Abelmoschus manihot flowers in treatment of kidney diseases. Phytother Res 2021; 35: 198-206.
[32] Chen JX, Fang QJ, Wan YG, Liu YL, Wang Y, Wu W, Tu Y, Wang MZ, Wang DG and Ge HT. Effects and mechanisms of total flavones of Abelmoschus manihot in inhibiting podocyte necroptosis and renal fibrosis in diabetic kidney disease. Zhongguo Zhong Yao Za Zhi 2023; 48: 4137-4146.
[33] Liu X, Zhang C, Fu Y, Dai J, Lu J, Liu G and Yang X. Huangkui capsule combined with finerenone attenuates diabetic nephropathy by regulating the JAK2/STAT3 signaling pathway based on network pharmacology, molecular docking, and experimental verification. Front Pharmacol 2025; 16: 1625286.
[34] Gu LF, Ge HT, Zhao L, Wang YJ, Zhang F, Tang HT, Cao ZY, Yu BY and Chai CZ. Huangkui capsule ameliorates renal fibrosis in a unilateral ureteral obstruction mouse model through TRPC6 dependent signaling pathways. Front Pharmacol 2020; 11: 996.
[35] Klar A, Baldassare M and Jessell TM. F-spondin: a gene expressed at high levels in the floor plate encodes a secreted protein that promotes neural cell adhesion and neurite extension. Cell 1992; 69: 95-110.
[36] Schubert D, Klar A, Park M, Dargusch R and Fischer WH. F-spondin promotes nerve precursor differentiation. J Neurochem 2006; 96: 444-453.
[37] Carrillo GL, Su J, Monavarfeshani A and Fox MA. F-spondin is essential for maintaining circadian rhythms. Front Neural Circuits 2018; 12: 13.
[38] Ho A and Südhof TC. Binding of F-spondin to amyloid-beta precursor protein: a candidate amyloid-beta precursor protein ligand that modulates amyloid-beta precursor protein cleavage. Proc Natl Acad Sci U S A 2004; 101: 2548-2553.
[39] Miyakawa R, Kobayashi M, Sugimoto K, Endo Y, Kojima M, Kobayashi Y, Furukawa S, Honda T, Watanabe T, Asano S, Soeda S, Hashimoto Y,

Fujimori K and Chiba H. SPON1 is an independent prognostic biomarker for ovarian cancer. J Ovarian Res 2023; 16: 95.

[40] Li H, Li J, Hu Y, Zhang R, Gu X, Wei Y, Zhang S, Chen X, Wei L, Li X, Gu S, Jin J, Huang H, Zhou H and Yang C. FOXO3 regulates Smad3 and Smad7 through SPON1 circular RNA to inhibit idiopathic pulmonary fibrosis. Int J Biol Sci 2023; 19: 3042-3056.

[41] Lovisa S, LeBleu VS, Tampe B, Sugimoto H, Vadnagara K, Carstens JL, Wu CC, Hagos Y, Burckhardt BC, Pentcheva-Hoang T, Nischal H, Allison JP, Zeisberg M and Kalluri R. Epithelial-to-mesenchymal transition induces cell cycle arrest and parenchymal damage in renal fibrosis. Nat Med 2015; 21: 998-1009.